Excitation functions for the reactions of Ar^+ with CH_4, CD_4, and CH_2D_2

J. R. Wyatt*, L. W. Strattan†, S. Chivalak, and P. M. Hierl

Department of Chemistry, University of Kansas, Lawrence, Kansas 66045
(Received 31 January 1975)

Integral reaction cross sections as a function of initial translational energy (0.4–30 eV c.m.) are reported for isotopic variants of the exoergic ion-molecule reaction $Ar^+ + CH_4 \rightarrow ArH^+ + CH_3$. The excitation functions, which maximize at about 5 eV and decrease at lower collision energies, appear to possess translational energy thresholds at about 0.1 eV. At the higher energies there is a large isotope effect favoring abstraction of H over D. The observed threshold behavior, unusual for exoergic reactions of positive ions, is discussed in terms of the formation of an $ArCH_4^+$ intermediate complex at low collision energies.

I. INTRODUCTION

Recently we studied the dynamics of the exothermic ($\Delta H = -1.7$ eV) ion–molecule reaction

$$Ar^+ + CH_4 \rightarrow ArH^+ + CH_3 \qquad (1)$$

at collision energies in the range 0.39–25 eV in the center of mass (c.m.).[1] The product velocity vector distributions were asymmetric about the c.m., indicating that the reaction is dominated by a direct mechanism over the energy range studied.[2] Although the spectator stripping model[3] approximates the dynamics of the reaction at collision energies less than 10 eV, the most probable translational energy (E'_{mp}) of the products was nearly 0.1 eV *lower* than the value predicted by this model. This observation is quite striking because it is the opposite of the behavior reported for a number of exoergic hydrogenic-transfer ion–molecule reactions.[4] We suggested[1] that this behavior may be caused by a basin in the potential energy hypersurface from which the reaction products can escape only with difficulty, particularly at the lowest collision energies. Extrapolation of E'_{mp} to low collision energy indicated that the stripping mechanism had a threshold at about 0.1 eV (c.m.), as had been suggested earlier by Henglein and co-workers.[5] Subsequent determination of the excitation function (integral reaction cross section as a function of collision energy) supported this suggestion. As communicated previously,[6] the excitation function for Reaction (1) maximizes at about 5 eV (c.m.) and decreases at lower collision energies, appearing to possess a threshold at about 0.1 eV.

We present here the details of those measurements, as well as new data on the excitation functions for the reactions

$$Ar^+ + CD_4 \rightarrow ArD^+ + CD_3, \qquad (2)$$

$$Ar^+ + CH_2D_2 \rightarrow ArH^+ + CHD_2 \qquad (3a)$$

$$\rightarrow ArD^+ + CH_2D. \qquad (3b)$$

II. EXPERIMENTAL

A. Apparatus

The instrument used in this study is a single beam-collision chamber type of chemical accelerator with product velocity and angular analysis. Ions, formed by electron impact, are focused into a nearly monoenergetic beam of variable energy (0.5–100 eV LAB) by a system of electrostatic lenses. This collimated beam passes through the collision chamber (see Fig. 1) containing the neutral target gas. The ion gun can be rotated about the center of the collision chamber, permitting the fixed detector to measure scattered products at various angles. Those ions leaving the collision chamber at the selected angle pass through a rectangular detection slit, a parallel plate retarding potential energy analyzer, and a set of strong focusing quadrupole lenses. Mass analysis of these ions is performed with a 30 cm, 90° deflection magnetic sector analyzer of a Nuclide mass spectrometer. The individual components of this instrument have been described in detail elsewhere.[7]

B. Internal states of the reactants

The Ar^+ is produced by impact of 40 eV electrons, so that the primary ion beam contains no doubly charged ions and less than 1% high energy metastable ions in the $^4D_{7/2}$, $^4F_{9/2}$, $^4F_{7/2}$, and $^2F_{7/2}$ states. Because of the selection rule for ΔJ, these metastable states should have lifetimes (with respect to the ground state of the ion) greater than 1 sec.[8] The flight time from the ion source to the collision chamber is less than 50 μsec. The remaining 99% of the Ar^+ ions are in the ^2P state and should be distributed statistically in a 2:1 ratio between the $J = 3/2$ and the $J = 1/2$ levels, which differ in energy by 0.18 eV.

The neutral target gas is assumed to be in thermal equilibrium with the walls of the collision chamber, so that the internal energy of the molecular reactant is determined by the temperature of the chamber (85 °C under the conditions of the experiment).

C. Multiplier gain

The ion detection system includes both an electron multiplier (16-stage, Be–Cu dynodes) and a Faraday cup which can be moved in front of the electron multiplier. The output from either detector is measured with a Nuclide Model EA-5 electrometer with EH-100 preamplifier head mounted near the detector. This electrometer system has a bandwidth of 5 kHz with a 10^8 Ω feedback resistor.

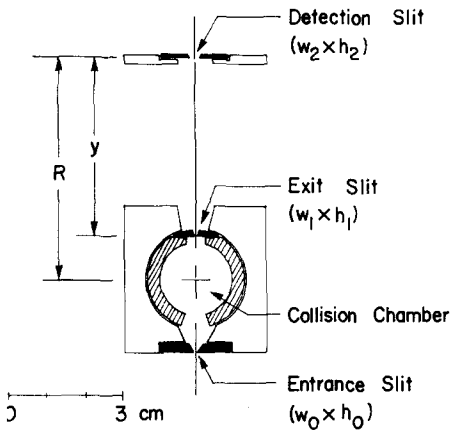

FIG. 1. Diagram of the collision chamber and detection aperture, shown in the plane defined by the incident ion beam and the axis of the detectors. Dimensions of the instrument used in the present study are given in Table I.

The gain k_i of the multiplier for a given ionic species i was determined by moving the Faraday cup collector in front of the electron multiplier and measuring the absolute ion intensity reaching the detector. The Faraday cup was then retracted and the multiplied signal measured. Product ion beams of sufficient intensity for accuract measurement with the Faraday cup were produced by admitting a mixture of Ar and H_2 (or D_2) directly into the ionization chamber. The pressure in this chamber could be raised sufficiently high that ArH^+ (or ArD^+) beams measuring 10^{-13} A or larger at the detector were produced by ion–molecule reactions in the primary ion source.

D. Target density

The target gas pressure (typically, 10^{-3} torr) was continuously monitored by an MKS Baratron Type 78M-XRSP pressure meter with a Type 78H-10SP sensor head connected directly to the collision chamber. Gas temperature was measured by a copper–constantan thermocouple in thermal contact with the collision chamber. The ideal gas law was used to calculate the target gas number density, n_B, from the measured pressure and temperature.

E. Data collection

Argon was admitted to the ionization chamber and a primary ion beam of moderate energy was produced. With the mass spectrometer high voltage held constant, the magnetic field was scanned manually until Ar^+ was detected. The primary ion beam energy was then set at the desired value, and the potentials on the electrostatic lenses of the ion gun were adjusted to give maximum beam intensity. The neutral target gas was then admitted to the collision chamber and the primary beam retuned, if necessary.

With the retarding potential of the energy analyzer set at zero for complete ion transmission, the angular distributions for the ions of interest were measured by rotating the ion source assembly about the center of the collision chamber while recording the ion intensity as a function of laboratory scattering angle Θ.

After the angular distributions of the primary and the product ions were determined, the apparatus was set to the angle of maximum intensity. The intensities of the ion signals, the gas pressure in the collision chamber, and the energy distribution of the primary ion beam were then measured.

III. CALCULATION

A. Evaluation of the geometrical factor $\int \Delta\Omega(x)dx$

Because the detector views a decreasing length $\Delta x(\Theta)$ of the collision path with increasing scattering angle, it is necessary to multiply the measured product ion intensity at each laboratory angle, $I_C(\Theta)_{\text{meas}}$, by a geometric factor $K(\Theta)$, so that the reported laboratory angular distributions $I_C(\Theta)$ will represent the relative ion intensity scattered into the solid angle $\Delta\Omega$ subtended by a detector of constant area, located at the laboratory angles Θ and Φ, from a reaction path of constant length L. That is,

$$I_C(\Theta) = K(\Theta) I_C(\Theta)_{\text{meas}}. \tag{4}$$

The geometric factor is given by

$$K(\Theta) = \frac{\int_L \Delta\Omega(x)dx}{\int_{\Delta x(\Theta)} \Delta\Omega(x)dx}, \tag{5}$$

where $\Delta\Omega(x)$ is the solid angle presented by the detector to particles scattered from position x along the collision path, and $\Delta x(\Theta)$ is that portion of the collision path viewed by the detector when it is set at the angle Θ. The integral $\int \Delta\Omega(x)\,dx$ has been evaluated for various types of detection apertures.[9]

For rectangular apertures as employed in the present study, and with the assumption that the projectile beam has negligible cross-sectional area, the numerator in Eq. (5) is given by

$$\int_L \Delta\Omega(x)\,dx = w_2 h_2 \int_{x_{\min}}^{x_{\max}} (R - x)^{-2} dx, \tag{6}$$

where w_2 and h_2 are width and height, respectively, of the detection slit which is located at a distance R from the center of the collision chamber, and where $x_{\min}$ and $x_{\max}$ are the distance of the entrance and exit slits to the collision chamber, respectively, measured from the center of the chamber.

We have obtained an expression for the integral $\int_{\Delta x(\Theta)} \Delta\Omega(x)\,dx$ that is exact for the simplifying assumptions of two-dimensional geometry and negligible beam-

TABLE I. Instrument dimensions.

$w_0 = w_1 = w_2$	1.0 mm
$h_0 = h_1$	1.5 mm
h_2	4.0 mm
R	57.2 mm
y	46.3 mm
$X_{\min}$	19.1 mm
$X_{\max}$	10.9 mm

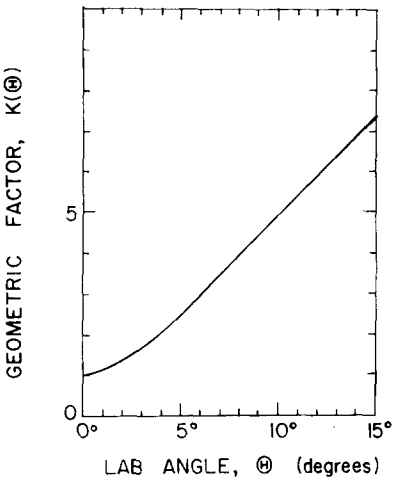

FIG. 2. Geometric correction factor $K(\Theta)$ vs laboratory scattering angle Θ. The correction factor was calculated from Eq. (5), using the dimensions given in Table I.

width[10] (see Fig. 2). For scattering angles greater than $\tan^{-1}[w_1/2(R-y)]$, about 2° in the present case, the exact expression is approximated very accurately by the expression first derived by Jordan and Brode:[11]

$$\int_{\Delta x(\Theta)} \Delta\Omega(x)\,dx \cong w_1 w_2 h_2/Ry \sin\Theta, \quad \text{if } \Theta \gg \tan^{-1}[w_1/2(R-y)]. \tag{7}$$

B. Calculation of the integral reaction cross section[12]

Because of the reactions studied in the present work have very small cross section (< 0.25 Å^2), production of adequate product ion intensity requires that the target gas density be increased to the extent that measurable attenuation of the primary ion beam occurs. Under these conditions, the integral reaction cross section σ_R is given by the following equation, the derivation of which appears in Appendix A:

$$\sigma_R = \frac{I_C/I_A}{n_B L} K(f, T), \tag{8}$$

where I_C is the total reactively scattered product ion intensity, I_A is the transmitted ion intensity, n_B is the number density of the target molecules, and L is the collision path length. The term $I_C/I_A\, n_B\, L$ is the familiar thin-target formula often used to calculate reaction cross sections, and the term

$$K(f, T) = \begin{cases} 1 & \text{if } f = 1 \\ [(f-1)\ln T]/(T^{f-1}-1) & \text{if } f \neq 1 \end{cases} \tag{9}$$

corrects for attenuation of the reactant and product beams (see Fig. 3). The transmission T is the ratio of the transmitted primary beam intensity to the incident primary beam intensity, I_A/I_A^0, and f is the ratio of the integral total cross section for attenuation of C by B to that for attenuation of A by B (i.e., $f = \sigma_{tot}^C/\sigma_{tot}^A$). For a given transmission T, the correction will be largest when $f = 0$. A situation approaching this limiting case is thought to exist in the present study. The integral total cross section for the attenuation of the reaction ion beam, σ_{tot}^A, appears to be dominated by the very large contribution from the various exothermic charge-exchange reactions between Ar^+ and CH_4.[1] Charge exchange between ArH^+ and CH_4, on the other hand, is endothermic. Since neutralization of ArH^+ is energetically forbidden, and since collision-induced dissociation is possible only at the higher collision energies, it is reasonable to assume that $\sigma_{tot}^C \ll \sigma_{tot}^A$ for the reactions under investigation. Consequently, with $f = 0$, the correction term is given by $K(0, T) = -T\ln T/(1-T)$.

Because both the primary and secondary ion beams are distributed over a solid angle greater than that subtended by the detector, the measured ion intensities at the angular maximum ($\Theta = 0°$, $\Phi = 0°$) represent only a fraction of the total ion flux leaving the collision chamber. Moreover, because their energy distribution is broader than that of the primary ions, the secondary ions may be discriminated against by the magnetic mass spectrometer (i.e., momentum analyzer), thus causing a relative broadening of the secondary ion mass peak. Additionally, the multiplier gain may be different for the primary and secondary ions. Consequently, the ratio of total ion currents, I_C/I_A, can be expressed in terms of the observed ion intensities at the angular maximum by the equation

$$\frac{I_C}{I_A} = \frac{K_C I_C(0°)}{K_A I_A(0°)} K_1 K_2, \tag{10}$$

where K_C and K_A correct for differences in collection efficiency caused by differences in angular distributions; $I_C(0°)$ and $I_A(0°)$ are the observed ion intensities at the angular maximum; K_1 corrects for differences in multiplier gain; and K_2 corrects for any broadening of the mass spectral peak of ions formed with a wide distribution of kinetic energies.

The quantities K_C and K_A were calculated from the measured angular distributions and simple geometric

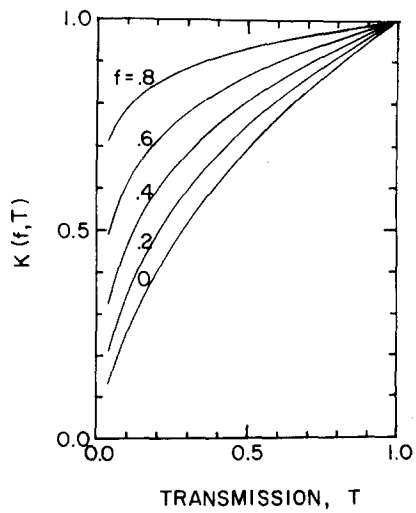

FIG. 3. Transmission correction factor $K(f, T)$ vs transmission T for various values of f. The factor $K(f, T)$ was calculated from Eq. (9).

considerations. By comparing the total ion intensity integrated over the entire plane of the detector with that portion contained within the small rectangular area subtended by the actual detection slit centered at the angular maximum, one obtains the factors K_C and K_A. That is,

$$K_C = \frac{\text{product ion intensity integrated over the entire detector plane}}{\text{product ion intensity integrated over area of detection slit}} .$$

The random orientation of initial impact parameters requires that the product distribution have cylindrical symmetry about the relative (i.e., primary ion) velocity vector.[2] Consequently, the angular distribution measured in one dimension, $I_C(\Theta)$, when rotated about the relative velocity vector will generate the two-dimensional angular distribution $I_C(\Theta, \Phi)$. A computer program was written which numerically integrates the observed angular distribution, corrected by the geometric factor $K(\Theta)$, over Θ and Φ.

As noted previously,[7] the calculation of this collection efficiency factor does not depend upon any assumptions concerning reaction mechanism, distribution about the center of mass, etc. It is only based upon measured angular distributions and the geometry of the detection system. Consequently, although the nomenclature is similar to that of Giese and Maier,[13] the procedure is actually equivalent to measuring the differential cross section in the laboratory system, $d^2\sigma(\Theta, \Phi)/d^2\Omega$, and integrating over the laboratory angles σ and Φ.[14]

The correction factor K_1 for differences in multiplier gain is given by

$$K_1 = k_A/k_C, \tag{11}$$

where k_A is the measured multiplier gain for the primary ion, and k_C is that for the product ion. The factor K_2 was determined by measuring the mass spectral peak shapes. After normalization to equal height, the areas were measured with a polar planimeter. The correction factor K_2 is then given by

$$K_2 = A_C/A_A, \tag{12}$$

where A_C and A_A are the measured peak areas for the product and reactant ions, respectively.

IV. RESULTS

A. Detection efficiencies

Multiplier gains were determined for Ar^+, ArH^+, and ArD^+ by the method described in Sec. II. C. The following results were obtained: for Ar^+/ArH^+, $K_1 = 0.99 \pm 0.01$; for Ar^+/ArD^+, $K_1 = 0.98 \pm 0.01$.

The correction factor K_2 was found to be unity when the mass spectrometer was operated at a resolving power $M/\Delta M$ of 500 and an accelerating voltage V of 2000 V. This is reasonable because ions of the same mass will be focused on the electron multiplier if their translational energy through the mass spectrometer is within the range $\Delta V = V(\Delta M/M) = 4$ eV, centered about the mean energy V. Direct measurement of the product-ion translational energy distributions[1] indicated that these distributions were never broader than about 2.5 eV.

B. Standard reactions

The desirability of validating an instrument's performance by demonstrating its "ability to reproduce the established behavior of certain standard reactions" has been emphasized.[15] We have previously reported[1] excitation functions, measured by the technique described in this paper, for the reactions

$$N_2^+ + H_2 \rightarrow N_2H^+ + H \tag{12'}$$

$$+ D_2 \rightarrow N_2D^+ + D. \tag{12''}$$

The results obtained agreed well with the data reported by several authors.[16–19]

In the present study, we have measured the excitation function for the reaction

$$Ar^+ + D_2 \rightarrow ArD^+ + D. \tag{13}$$

The selection of Reaction (13) as a standard has two advantages. First, this reaction is one of the more thoroughly studied ion–molecule reactions, and there now exits reasonable agreement on the absolute value of the integral reaction cross section over a wide range of energies. Second, at a given Ar^+ energy, the laboratory angular and velocity distributions of the ArD^+ produced in Reactions (2) and (3b) are nearly identical to those of the ArD^+ from Reaction (13); hence, our determination of collection efficiencies and cross sections for (2) and (3b) should be of an accuracy similar to that obtained for (13).

The data obtained for Reaction (13) are summarized in Table II. The cross sections listed were calculated from the thin-target formula, $\sigma_R = I_C/I_A n_B L$, rather than from the exact expression given by Eq. (8). Because of

TABLE II. Integral cross sections for the reaction $Ar^+ + D_2 \rightarrow ArD^+ + D$.

Most probable lab energy of Ar^+ E_{LAB}(eV)	Most probable relative energy E(eV)	Relative collection efficiency K_C/K_A	Integral reaction cross section $\sigma_R(10^{-16}$ cm$^2)$
1.75	0.16	6.52	31.6
2.44	0.22	4.86	35.7
3.09	0.28	7.23	41.1
7.40	0.67	4.65	17.7
10.55	0.96	3.39	14.5
18.56	1.69	4.46	5.97
25.99	2.36	2.74	4.45
35.00	3.18	1.58	2.46
51.30	4.66	1.77	2.37
51.30	4.66	1.62	1.96
60.30	5.48	1.31	0.64
78.80	7.16	3.56	0.56

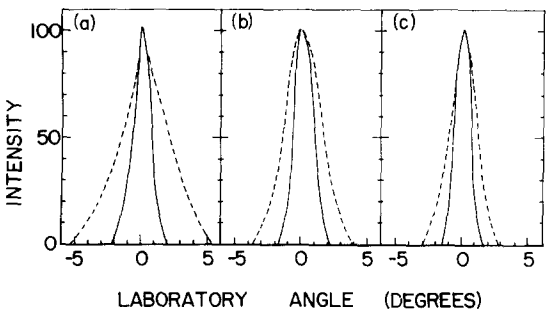

FIG. 4. Typical laboratory angular distributions for the reaction $Ar^+ + CD_4 \rightarrow ArD^+ + CD_3$. The solid line represents the observed laboratory angular distribution for the reactant ion. The dashed line represents the laboratory angular distribution of the ionic product $I_C(\Theta)$; i.e., the observed product intensity multiplied by the geometric factor $K(\Theta)$. The intensities have been normalized to 100 at the angular maximum. Data are shown for three Ar^+ beam energies; E_{LAB}: (a) 1.80 eV; (b) 6.04 eV; and (c) 34.96 eV.

the large cross section for this reaction, adequate product intensity could be produced by using low target gas density, thereby causing little attenuation of the primary beam and a correction factor $K(f, T)$ near unity. The measured cross sections for Reaction (13) are depicted graphically in Fig. 5, where the present results are compared with data from other laboratories.[17-19]

C. The reactions Ar^+ with CH_4, CD_4, and CH_2D_2

Typical one-dimensional angular distributions, $I(\Theta)$, are shown in Fig. 4 for the reactant and the product ions of Reaction (2) at several laboratory energies of the reactant ion.

The cross section data for Reactions (1)–(3) are summarized in Table III. E_{LAB} represents the most probable value of the translational energy of the primary ion in the laboratory coordinate system, as determined by differentiation of the ion intensity vs retarding potential curve. Ignoring the thermal motion of the neutral target, the most probable collision energy, E, in the center-of-mass coordinate system is given by

$$E = \frac{m_A}{m_A + m_B} E_{LAB}, \tag{14}$$

where m_A and m_B are the masses of the ionic and the neutral reactant, respectively. The correction factors for differences in the primary and secondary ion angular distributions, K_C/K_A, were calculated by integration of the observed laboratory distributions—such as those shown in Fig. 4—by the method described in Sec. III. B. Correction factors for attenuation of the primary ion beam, $K(0, T)$ have been calculated from Eq. (9) under the assumption that $f = 0$. The transmission T at each energy was determined by measuring the primary ion intensity before (I_A^0) and after (I_A) admission of the target gas to the collision chamber. The integral reaction cross sections σ_R were calculated from Eq. (8). The excitation functions (σ_R vs E) for Reactions (1)–(3) are plotted in Figs. 6 and 7.

It was found that the over-all shape of the excitation functions for Reactions (1)–(3) could be described reasonably well (see Figs. 6 and 7) by a simple expression of the general form

$$\sigma_R(E) = \begin{cases} 0 & \text{if } E \leq E_0 \\ A(E - E_0)^B e^{-C(E-E_0)} & \text{if } E > E_0, \end{cases} \tag{15}$$

where E_0 is the apparent translational energy threshold (taken as 0.1 eV); E is the relative translational energy; and A, B, and C are parameters chosen to provide the best fit to the experimental data. It must be emphasized that no theoretical significance whatsoever is attached to Eq. (15); it simply provides a convenient function which summarizes a quantity of experimental data. The "best" values of the parameters A, B, and C, determined by a least squares analysis of the data, are listed in Table IV for each reaction. These values were used to calculate the excitation functions shown by the solid lines in Figs. 6 and 7.

The probability $p_a(E)$ that abstraction occurs in a collision at relative energy E can be taken as the ratio of the reaction cross section to the total cross section:

$$P_a(E) = \frac{\sigma_R(E)}{\sigma_{tot}(E)}. \tag{16}$$

Values of the abstraction probability $p_a(E)$ have been calculated from the data in Table III for Reactions (1) and (2). It was found that the results could be described by the expression $p_a(E) = A'(E - E_0)^{B'} e^{-C'(E-E_0)}$ when $E \geq E_0$. The parameters, determined by a least squares analysis, are listed in Table IV, and the resulting analytic expressions are plotted in Fig. 8.

D. Experimental uncertainty

The pressure of the neutral target gas, as measured by the MKS Baratron pressure gauge, is estimated to

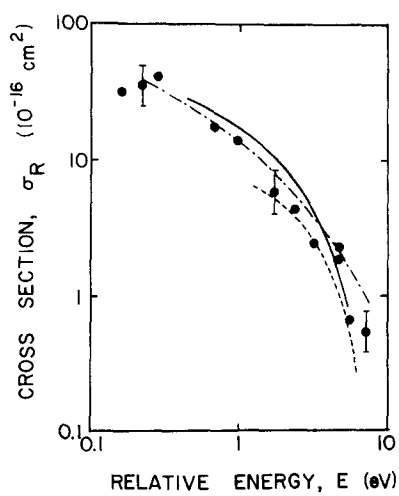

FIG. 5. Integral reaction cross section σ_R vs initial relative translational energy E for the reaction $Ar^+ + D_2 \rightarrow ArD^+ + D$. The closed circles represent the results obtained in the present study (Table II). Estimated limits of experimental uncertainty are indicated by error bars for several of the points. Experimental results of other authors are included: ---, Hyatt and Lacmann[17]; —, Homer *et al.*[18]; ---, Lacmann and Henglein.[19]

TABLE III. Integral cross sections for reactions of the type $Ar^+ + CY_4 \rightarrow ArY^+ + CY_3$.

Most probable lab energy of Ar^+ E_{LAB} (eV)	Most probable relative energy E (eV)	Pressure of CY_4 (10^{-3} torr)	Relative collection efficiencies K_C/K_A [a]	Transmission factor $K(0,T)$ [b]	Integral reaction cross section σ_R (10^{-16} cm^2) [c]
A. $Ar^+ + CH_4 \rightarrow ArH^+ + CH_3$					
1.41	0.40	1.00	1.70	0.455	0.049
2.22	0.63	1.11	1.70	0.467	0.065
2.74	0.78	1.13	2.15	0.480	0.065
3.90	1.11	1.15	1.49	0.506	0.103
4.05	1.16	1.30	1.99	0.517	0.091
4.76	1.36	1.03	1.86	0.553	0.097
6.76	1.93	1.00	1.93	0.655	0.142
6.92	1.98	1.58	2.57	0.678	0.182
7.47	2.13	1.40	2.10	0.695	0.202
9.95	2.84	1.51	2.37	0.733	0.232
14.2	4.07	1.52	1.74	0.773	0.240
14.4	4.11	1.11	1.50	0.773	0.218
20.0	5.70	1.52	1.35	0.790	0.186
25.0	7.14	1.58	1.34	0.792	0.173
30.0	8.57	1.48	1.32	0.797	0.143
30.0	8.57	1.05	1.38	0.795	0.169
35.0	10.0	1.25	1.32	0.795	0.169
39.8	11.4	1.60	1.26	0.799	0.122
39.8	11.4	1.08	1.28	0.801	0.095
45.5	12.8	1.50	1.33	0.803	0.128
55.3	15.8	1.00	1.50	0.811	0.074
75.7	21.4	1.11	1.19	0.818	0.031
97.3	27.8	1.10	1.20	0.826	0.013
B. $Ar^+ + CD_4 \rightarrow ArD^+ + CD_3$					
1.20	0.40	1.35	3.05	0.480	0.045
1.80	0.60	1.18	3.05	0.493	0.074
1.97	0.66	0.96	3.05	0.493	0.077
2.40	0.80	1.24	3.05	0.506	0.080
2.89	0.96	0.78	3.05	0.520	0.071
3.60	1.20	1.01	2.00	0.534	0.078
4.20	1.40	1.00	3.43	0.562	0.075
4.56	1.52	1.06	1.88	0.577	0.096
6.04	2.01	1.42	1.78	0.671	0.115
11.1	3.68	1.25	1.79	0.773	0.140
12.7	4.23	1.45	1.45	0.780	0.094
16.2	5.41	1.05	1.25	0.788	0.087
18.5	6.17	0.52	1.08	0.792	0.080
22.7	7.55	0.70	1.33	0.795	0.080
26.5	8.82	0.81	1.08	0.795	0.028
30.7	10.2	0.82	1.57	0.795	0.020
31.8	10.6	0.88	1.66	0.795	0.025
34.9	11.7	0.90	1.81	0.799	0.021
38.1	12.7	0.96	1.29	0.803	0.018
45.3	15.1	0.95	1.01	0.807	0.004
50.5	16.8	0.85	1.26	0.807	0.009
C. $Ar^+ + CH_2D_2 \rightarrow ArH^+ + CHD_2$					
1.60	0.50	1.18	1.69	0.414	0.034
2.35	0.73	1.42	1.67	0.352	0.027
2.95	0.92	0.95	1.35	0.525	0.051
4.20	1.30	1.12	1.22	0.521	0.033
4.80	1.49	0.89	1.20	0.629	0.043
6.10	1.89	0.90	1.45	0.685	0.050
7.20	2.23	1.04	1.30	0.677	0.068
7.78	2.41	0.78	1.48	0.764	0.095
8.51	2.64	0.90	1.49	0.738	0.085
13.0	4.03	1.20	1.34	0.724	0.100
16.1	5.01	1.10	1.11	0.777	0.076
21.5	6.66	1.15	1.06	0.776	0.078
24.3	7.54	1.35	1.17	0.746	0.093
29.6	9.20	1.07	1.16	0.802	0.087

TABLE III. (*Continued*)

Most probable lab energy of Ar^+ E_{LAB}(eV)	Most probable relative energy E(eV)	Pressure of CY_4 (10^{-3} torr)	Relative collection efficiencies K_C/K_A [a]	Transmission factor $K(0,T)$[b]	Integral reaction cross section $\sigma_R(10^{-16}$ cm^2)[c]
C. $Ar^+ + CH_2D_2 \rightarrow ArH^+ + CHD_2$					
51.5	16.0	1.04	1.50	0.820	0.053
60.6	18.8	1.04	1.30	0.824	0.030
80.1	24.9	1.04	1.20	0.828	0.017
99.0	30.8	1.04	1.20	0.832	0.002
D. $Ar^+ + CH_2D_2 \rightarrow ArD^+ + CH_2D$					
1.60	0.50	1.18	2.07	0.414	0.010
1.80	0.56	0.94	1.55	0.293	0.011
2.35	0.73	1.42	2.15	0.352	0.013
2.95	0.92	0.95	1.64	0.525	0.015
4.20	1.30	1.12	1.92	0.521	0.022
4.30	1.33	0.85	1.92	0.622	0.039
6.10	1.89	0.90	1.64	0.685	0.057
8.51	2.64	0.90	1.91	0.738	0.071
13.0	4.03	1.20	1.40	0.724	0.064
16.1	5.01	1.10	1.31	0.777	0.030
21.5	6.66	1.15	1.04	0.776	0.021
24.3	7.54	1.35	1.10	0.746	0.022
29.6	9.20	1.07	1.19	0.802	0.019
51.5	16.0	1.04	1.84	0.820	0.004
60.6	18.8	1.04	1.25	0.824	0.001
80.1	24.9	1.04	1.0	0.828	0.000
99.0	30.8	1.04	1.0	0.832	0.000

[a]Ratio of collection efficiency correction factors (see Sec. III. B).
[b]Correction factor for attenuation of primary beam, calculated from Eq. (9) with $f=0$.
[c]Integral reaction cross section, calculated from Eqs. (8) and (10).

be uncertain by 5%,[15] while the temperature measurement is probably reliable to within 2%. Inhomogeneities in gas density near the entrance and exit slits of the collision chamber cause an uncertainty in the length of the collision region that is estimated to be about 3%, the ratio of slitwidth to nominal collision path length. The ratio $I_C(0°)/I_A(0°)$ may be in error by as much as 10%, primarily because of the relatively low signal-to-noise ratio resulting from the low intensity of the product ion signal. The correction factors K_1 and K_2 are reliable to within 1%, but the relative collection efficiency ratio, K_C/K_A, is estimated to have an uncertainty of about 20%, again due primarily to statistical fluctuation in the product ion intensity, especially at the larger scattering angles. Therefore, the values reported for the integral reaction cross sections are probably reliable to within about ± 40%.

Moreover, the assumption that the parameter f equals zero may introduce a systematic error, the magnitude of which will depend upon the transmission T for each experiment. Since, for a given T, the term $K(f, T)$ will have its minimum value when $f=0$, the reported integral reaction cross sections must be considered as lower limits to the actual cross sections, while the upper limit will be given by the thin-target formula.

Each reported Ar^+ laborabory energy corresponds to the maximum in the Ar^+ energy distribution, determined by retarding potential analysis, and is probably accurate to within a few percent. About this most probable value, there is a distribution of Ar^+ energies, the full-width at half-maximum of the distribution being $0.013\ E_{LAB} + 0.15$

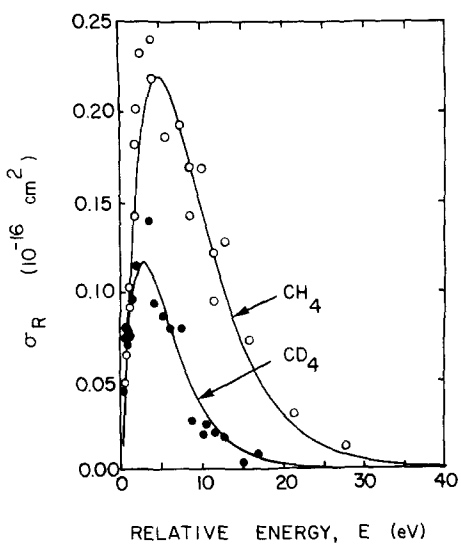

FIG. 6. Integral reaction cross sections σ_R vs initial relative translational energy E for the reaction $Ar^+ + CH_4 \rightarrow ArD^+ + CH_3$ (○) and $Ar^+ + CD_4 \rightarrow ArD^+ + CD_3$ (●). The values of the cross sections, calculated from Eqs. (8) and (10), are listed Table III. The solid lines represent an empirical fit [Eq. (15)] to the experimental data, using the parameters given in Table IV.

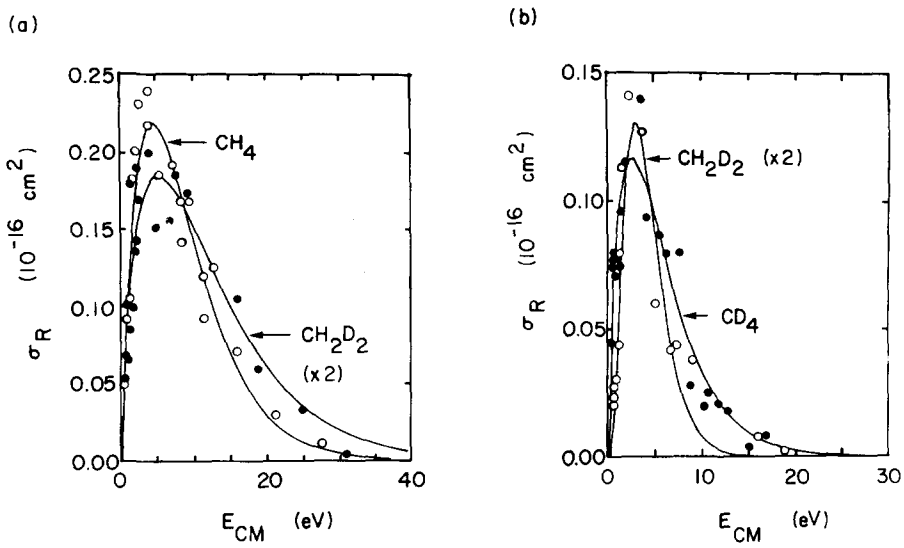

FIG. 7. Integral reaction cross section σ_R vs initial relative translational energy E for the formation of (a) ArH^+ from CH_4 (○) and from CH_2D_2 (○); (b) ArD^+ from CD_4 (●) and from CH_2D_2. The cross sections for the reactions with CH_2D_2 have been doubled to allow direct comparison on the basis of yield per C–H or C–D bond. The solid lines represent an empirical fit [Eq. (15)], using the parameters listed in Table IV.

eV. This spread in beam energies and the thermal motion of the target molecules will smear out any fine structure in the excitation function and may cause the experimentally determined threshold to be somewhat lower than the actual translational energy threshold (see Ref. 15). No attempt was made in the present study to deconvolute the experimental cross sections to remove the effect of target motion and beam spread.

V. DISCUSSION

A. Standard reactions

As shown in Fig. 5, the integral cross sections for Reaction (13) determined in the present study agree quite well with the values reported by other laboratories. This agreement implies that the method employed to determine absolute reaction cross sections in this study contains no serious systematic errors, and that similar accuracy might be expected for other reactions which yield ionic products whose laboratory velocity vector distributions are similar to those produced in Reaction (13). Reactions (1)–(3), whose dynamics are reasonably approximated by the spectator stripping model,[1] are in this category.

B. Reactions of Ar^+ with CH_4, CD_4, and CH_2D_2

The excitation functions for Reactions (1)–(3) have three interesting features: (1) The cross sections for these reactions are approximately 100 times smaller than those for the corresponding reactions with molecular hydrogen. (2) The excitation functions for these exothermic ion–molecule reactions appear to possess a translational energy threshold. (3) There is a large iostope effect favoring formation of ArH^+ over ArD^+.

The small cross section for the abstraction of atomic hydrogen from methane by Ar^+ has been remarked upon previously.[20,21] This is presumed to be a result of competition from the very fast dissociative charge transfer reactions that occur in the Ar^+–CH_4 system.[22,23]

The observation that the excitation functions for these reactions maximize at about 5 eV (c.m.) and decrease at lower collision energies, appearing to possess thresholds at about 0.1 eV, is most uncommon behavior for exothermic ion–molecule reactions. Excitation functions of this shape are normally associated with endoergic ion–molecule reactions, such as $C^+(H_2, H)CH^+$.[24,25] It has long been thought that exoergic reactions of positive ions have no activation energy,[26] although the reaction $O^+(N_2, N)NO^+$ is one well known exception[27] to this generalization.

A plausible explanation might, at first, appear to be that ArH^+ is produced by the reaction of Ar^+ in an electronically excited state whose lifetime τ is comparable in magnitude to the flight time from the ion source to the collision chamber. At the higher beam energies (>5 eV c.m.), the flight time is sufficiently short relative to τ that nearly all of the electronically excited Ar^+ ions reach the collision chamber and can react, whereas the flight time for low energy (<1 eV c.m.) beams is long enough that most of the electronically excited Ar^+ has lost the excitation energy necessary for reaction. However, the ionization efficiency curve for ArH^+ production[20] clearly shows that ArH^+ appears at the same voltage as ground state Ar^+. Consequently, the observed threshold behavior in the excitation function cannot be attributed to the reaction of electronically excited Ar^+.

TABLE IV. Parameters for the excitation function and the abstraction probability.[a]

Reaction	A	B	C	A'	B'	C'
(1)	0.133	1.01	0.226	0.00131	1.46	0.257
(2)	0.121	0.835	0.321	0.00104	1.89	0.492
(3a)	0.057	0.740	0.142	•••	•••	•••
(3b)	0.052	2.57	0.861	•••	•••	•••

[a]The excitation function is assumed to be given by the expression $\sigma_R(E) = A(E-E_0)^B e^{-C(E-E_0)}$ and the abstraction probability by $P_a(E) = A'(E-E_0)^{B'} e^{-C'(E-E_0)}$. The parameters were determined by a least squares analysis of the experimental data.

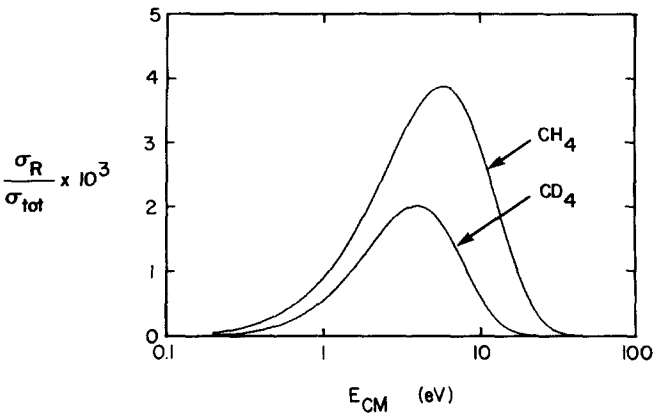

FIG. 8. Reaction probability σ_R/σ_{tot} vs initial relative translational energy E for the reactions $Ar^+ + CH_4 \rightarrow ArH^+ + CH_3$ and $Ar^+ + CD_4 \rightarrow ArD^+ + CD_3$. The solid lines represent an empirical fit (see Sec. IV.C) to the experimental data (not shown), using the parameters listed in Table IV.

As discussed previously,[1] the measured product angular and velocity distributions suggest that the potential-energy hypersurfaces for Reactions (1)–(3) possess a basin. (The observation of $ArCH_4^+$ in high-pressure mass spectrometric studies[20] of argon–methane mixtures supports this suggestion.) Although the abstraction reaction is dominated by a direct mechanism over the entire energy range studied,[1] the dynamics indicate that the stripping mechanism has a translational energy threshold at about 0.1 eV; at lower collision energies, the products do not retain sufficient momentum to escape the basin and separate completely in a direct manner (i.e., without "backtracking").[28] Failing to separate, the nascent products will oscillate in the vicinity of the potential minimum until they either (1) reform the reactants, (2) exit via another reaction channel (e.g., charge exchange), or (3) undergo a secondary encounter that produces sufficient vibrational–translational energy transfer to effect separation. The decrease in the reaction cross section at low energy and the asymmetry of the product velocity vector distributions indicate that the $ArCH_4^+$ intermediate preferentially decomposes via reaction channels other than ArH^+ formation.

An isotope effect favoring abstraction of H atoms rather than D atoms occurs both intermolecularly with CH_4 and CD_4 and intramolecularly with CH_2D_2 (see Figs. 6 and 7). Although this effect is operative over the entire energy range studied, it is most pronounced at the higher collision energies ($E > 5$ eV), where the cross section for H-atom abstraction is more than an order of magnitude greater than that for D-atom abstraction. Similar isotope effect have been reported[29] for the reaction of N_2^+ with CH_4 and CD_4 at collision energies greater than 9 eV (c.m.).

When compared on the basis of yield per C–H or C–D bond, the cross sections for Reactions (3a) and (3b) are approximately equal to those for Reactions (1) and (2), respectively (see Fig. 7). This finding indicates that the isotopic differences in abstraction arise principally from a primary isotope effect caused by the difference in mass of the abstracted atom.[30] Primary isotope effects caused by the difficulty of product stabilization in high energy collisions have been discussed in terms of the spectator-stripping model, which predicts that the cross sections for isotopic variants of a given reaction should be equal at the same value of E_a, the energy of the projectile relative to the atom it abstracts.[31] While this predicted behavior has been observed for ionic reactions with H_2, HD, and D_2, the present results and those of Mahan and co-workers[29] indicate such agreement does not occur in abstraction from the isotopic methanes. Presumably, the additional degrees of freedom available in the neutral methyl fragment assist stabilization of the ionic product at the higher collision energies, thereby reducing the energy and momentum constraints existing in the case of molecular hydrogen.

The isotopic preference for abstraction of H rather than D is a familiar feature of the reactions of recoil tritium atoms with various organic molecules.[32] An HT/DT ratio of 1.4, for example, has been reported for the reaction of hot tritium with CH_2D_2.[33] In these bulk experiments, collisions occur over a wide range of energies, and the product yield is proportional to the "reactivity integral," I, given by the area under the abstraction probability, $P_a(E)$, plotted against $\ln E$.[32] The data shown in Fig. 8 indicate that a product ratio ArH^+/ArD^+ of about 2.0 would have been obtained if Reactions (1) and (2) had been studied under the conditions of a hot atom experiment. Although somewhat greater in magnitude than the effect observed in the reactions of recoil tritirum, the present results indicate that such isotope effects are probably common to most reactions, both ionic and neutral, occurring at high translational energies. The origins of these isotopic differences are poorly understood at this time. It is hoped, however, that they will become better understood as excitation functions become available for various reactions over a range of collision energies.

ACKNOWLEDGMENTS

Acknowledgment is made to the donors of the Petroleum Research Fund, administered by the American Chemical Society, for partial support of this research. Additional support was provided by the Research Corporation and by the University of Kansas General Research Fund.

APPENDIX: MEASUREMENT OF THE INTEGRAL REACTION CROSS SECTION[12]

Consider a beam of particles A passing through a target gas B, with which they may react to yield products C + D. Per unit scattering length, dx, the increase in the intensity of C is given by

$$dI_C = I_A \sigma_R n_B dx - I_C \sigma_{tot}^C n_B dx, \tag{A1}$$

where I_A and I_C are the intensities of A and C, respectively, at point x, σ_R is the integral cross section for the reaction $A + B \rightarrow C + D$, σ_{tot}^C is the integral total cross section for the attenuation of C by B, and n_B is the number density of the target gas. Similarly, the change in intensity of the reactant beam is given by

$$dI_A = I_C \sigma_R^{C\to A} n_B dx - I_A \sigma_{tot}^A n_B dx, \quad \text{(A2)}$$

where $\sigma_R^{C\to A}$ represents the integral cross section for the collision-induced dissociation of C to regenerate A, and where σ_{tot}^A is the integral total cross section for the attenuation of A by B.

To a good approximation, $I_C \sigma_R^{C\to A} \ll I_A \sigma_{tot}^A$. Neglecting, therefore, the first term on the right hand side of Eq. (5) and assuming n_B is independent of x, integration of the resulting expression over L, the length of the collision path, yields the familiar result

$$I_A = I_A^0 \exp(-\sigma_{tot}^A n_B L), \quad \text{(A3)}$$

where I_A^0 is the unattenuated intensity of A and I_A is the transmitted intensity.

Substitution of this expression into Eq. (A1) yields

$$dI_C = I_A^0 \sigma_R n_B \exp(-\sigma_{tot}^A n_B L) dx - I_C \sigma_{tot}^C n_B dx. \quad \text{(A4)}$$

This linear differential equation of the first order can be solved by the method of Laplace transforms.[34] For the general case ($\sigma_{tot}^A \neq \sigma_{tot}^C$), the result is

$$I_C = \frac{\sigma_R I_A^0}{\sigma_{tot}^A - \sigma_{tot}^C} \exp(-\sigma_{tot}^C n_B L) - \exp(-\sigma_{tot}^A n_B L) . \quad \text{(A5)}$$

The cross sections σ_{tot}^A and σ_{tot}^C can, in principle, be obtained by measuring the attenuation of beams of A and of C, respectively, passing through B. A simpler although perhaps less exact method is to assume that the integral total cross section for attenuation of C is some fraction f of that for attenuation of A; i.e., that $\sigma_{tot}^C = f\sigma_{tot}^A$. Solving Eq. (A5) for the integral reaction cross section then yields the result

$$\sigma_R = \frac{I_C}{I_A n_B L} \frac{(f-1)\ln T}{T^{(f-1)} - 1}, \quad \text{(A6)}$$

where $T = I_A/I_A^0 = \exp(-\sigma_{tot}^A n_B L)$, the transmission. The term $I_C/I_A n_B L$ is the familiar thin-target formula often used to calculate reaction cross sections, and $K(f, T) = (f-1)\ln T/(T^{f-1} - 1)$ is the correction factor that accounts for attenuation of reactant and produce beams.

A special situation occurs if $\sigma_{tot}^A = \sigma_{tot}^C$. In this case, the solution to Eq. (7) takes the form

$$I_C = I_A^0 \sigma_R n_B L \exp(-\sigma_{tot}^A n_B L) = I_A n_B L \sigma_R \quad \text{(A7)}$$

or, $\sigma_R = I_C/I_A n_B L$, the thin-target formula.

*Present address: Naval Research Laboratory, Washington, D.C. 20375.

†Present address: Department of Chemistry, Emory University, Atlanta, GA.

[1] J. R. Wyatt, L. W. Strattan, S. C. Snyder, and P. M. Hierl, "Chemical Accelerator Studies of Reaction Dynamics. $Ar^+ + CH_4 \rightarrow ArH^+ + CH_3$" (submitted to J. Chem. Phys.).

[2] D. R. Herschbach, Discuss. Faraday Soc. 33, 149 (1962).

[3] A. Henglein, K. Lacmann, and G. Jacobs, Ber. Bunsenges. Phys. Chem. 69, 286, 292 (1965).

[4] (a) J. L. Franklin and M. A. Haney, J. Phys. Chem. 73, 2857 (1969); (b) C. M. Connally and E. A. Gislason, Chem. Phys. Lett. 14, 103 (1972), and references cited therein.

[5] H. Mittman, H. P. Weise, A. Ding, and A. Henglein, Z. Naturforsch. A 26, 1112 (1971).

[6] J. R. Wyatt, L. W. Strattan, S. C. Snyder, and P. M. Hierl, J. Chem. Phys. 60, 3702 (1974).

[7] P. M. Hierl, L. W. Strattan, and J. R. Wyatt, Int. J. Mass Spectrom. Ion Phys. 10, 385 (1973).

[8] H. D. Hagstrum, Phys. Rev. 104, 309 (1956).

[9] See, for example, C. E. Kuyatt, in *Methods of Experimental Physics*, edited by B. Bederson and W. L. Fite (Academic, New York, 1968), Vol. 7, Part A, pp. 1–115.

[10] The influence of the slit heights on the calculation of the geometric factor has recently been considered by I. Sauers and E. W. Thomas, Rev. Sci. Instrum. 45, 809 (1974). This refinement has a negligible effect upon $K(\Theta)$.

[11] E. B. Jordan and R. B. Brode, Phys. Rev. 43, 112 (1933).

[12] The nomenclature used here is that of H. Pauly and J. P. Toennies, in *Advances in Atomic and Molecular Physics*, edited by D. R. Bates and I. Estermann (Academic, New York, 1965), Vol. 1, pp. 195–344.

[13] C. F. Giese and W. B. Maier, II, J. Chem. Phys. 39, 739 (1963).

[14] See, for example, M. E. Gersh and R. B. Bernstien, J. Chem. Phys. 56, 6131 (1972).

[15] M. Henchman, in *Ion-Molecule Reactions*, edited by J. L. Franklin (Plenum, New York, 1972), Vol. 1, pp. 101–259.

[16] B. R. Turner, M. A. Fineman, and R. F. Stebbings, J. Chem. Phys. 42, 4088 (1965).

[17] D. Hyatt and K. Lacmann, Z. Naturforsch. A 23, 2080 (1968).

[18] J. B. Homer, R. S. Lehrle, J. C. Robb, and D. W. Thomas, Adv. Mass Spectrom. 3, 415 (1966).

[19] K. Lacmann and A. Henglein, Ber. Bunsenges. Phys. Chem. 69, 286 (1965).

[20] F. H. Field, H. N. Head, and J. L. Franklin, J. Am. Chem. Soc. 84, 1118 (1962).

[21] A. Ding, A. Henglein, D. Hyatt, and K. Lacmann, Z. Naturforsch. A 23, 2084 (1968).

[22] V. L. Talrose and G. V. Karachevtsev, Adv. Mass Spectrom. 3, 211 (1966).

[23] A. J. Masson, K. Birkinshaw, and M. J. Henchman, J. Chem. Phys. 50, 4112 (1969).

[24] W. B. Maier, II, J. Chem. Phys. 46, 4991 (1967).

[25] E. Lindemann, L. C. Frees, R. W. Rozett, and W. S. Koski, J. Chem. Phys. 56, 1003 (1972).

[26] F. W. Lampe, J. L. Franklin, and F. H. Field, Prog. React. Kinet. 1, 84 (1961).

[27] A. Pipano and J. J. Kaufman, J. Chem. Phys. 56, 5258 (1972).

[28] J. C. Polanyi, Discuss. Faraday Soc. 44, 293 (1967).

[29] E. A. Gislason, B. H. Mahan, C.-W. Tsao, and A. S. Werner, J. Chem. Phys. 50, 142 (1969).

[30] Rigorously, cross sections for ArH^+ formation from CD_3H and for ArD^+ formation from CH_3D should have been compared with those for Reactions (1) and (2) in order to separate completely primary and secondary isotope effects. However, the further diminution this would cause in the already low product ion intensity precluded such an experiment at this time.

[31] A. Henglein, Adv. Chem. Ser. 58, 63 (1966).

[32] See, for example, R. Wolfgang, Prog. React. Kinet. 3, 97 (1965).

[33] J. K. Lee, B. Musgrave, and F. S. Rowland, J. Phys. Chem. 64, 1950 (1960).

[34] See, for example, W. T. Martin and E. Reissner, *Elementary Differential Equations* (Addison-Wesley, Reading, MA, 1956), pp. 127–133.